Applied Catalysis B: Environmental 191 (2016) 116–129

Contents lists available at ScienceDirect

Applied Catalysis B: Environmental

journal homepage: www.elsevier.com/locate/apcatb

DOC modeling combining kinetics and mass transfer using inert washcoat layers

Björn Lundberg[a], Jonas Sjöblom[b], Åsa Johansson[c], Björn Westerberg[d], Derek Creaser[a,*]

[a] Department of Chemistry and Chemical Engineering, Chemical Reaction Engineering, Chalmers University of Technology, Göteborg SE-412 96, Sweden
[b] Department of Applied Mechanics, Division of Combustion, Chalmers University of Technology, Göteborg SE-412 96, Sweden
[c] Johnson Matthey AB, Västra Frölunda SE-421 31, Sweden
[d] Scania AB, Södertälje SE-151 87, Sweden

ARTICLE INFO

Article history:
Received 28 November 2015
Received in revised form 21 February 2016
Accepted 12 March 2016
Available online 15 March 2016

Keywords:
Diesel oxidation catalyst
Transport resistances
Inhibition effects
Kinetic modeling

ABSTRACT

The aim of this study was to develop a kinetic and transport model for diesel oxidation catalysts (DOC) with a satisfactory compromise between accuracy and computational demands for robust simulation of transient full-scale operation. Specifically the model accounts for surface concentrations of key species needed to capture transient features for typical lean exhaust conditions. In addition, the model accounts for transport limitations and distinguish them from reaction kinetics as well as apparent NO oxidation inhibition effects due to reactions. To achieve this, lab scale experiments were performed with DOCs with different platinum loadings and three different washcoat configurations of which two had an inert top layer. Both kinetic parameters for a detailed kinetic model and effective diffusivities were optimized for the experimental data using a single channel catalyst model. The experiments showed a clear effect of increased transport resistance for propene and CO and also that NO_2 plays an important role as an oxidizing agent for preferentially CO at low temperature (<120 °C). The resulting model showed good agreement with measurement data using O, CO and NO_2 as the only surface species. The use of different thicknesses of an inert washcoat layer closest to the gas bulk aided the resolution of kinetics from transport phenomena.

1. Introduction

The diesel oxidation catalyst (DOC) is an indispensable part of the aftertreatment system of heavy duty diesel engines that has been in use since the 1990s. The role of the DOC is to utilize the oxygen excess of the lean burn engine to oxidize CO and hydrocarbons (HC) to CO_2 and to oxidize NO to NO_2. Generally the DOC is placed first in the aftertreatment system which means that its performance also is of utmost importance for downstream components such as the selective catalytic reduction (SCR) catalyst and the diesel particulate filter (DPF). Strengthened emission standards are continuously increasing the demands on aftertreatment performance and to meet these demands mathematical models of the DOC can be an important tool in system design, optimization and providing increased insight in component operation.

When a mathematical model of a catalytic converter is derived it is important to consider the effects of both reaction kinetics and transport phenomena. The kinetics determine the rate at which the components are consumed or produced as a function of temperature, concentration, and surface coverages. Transport phenomena control the transport of heat, mass and momentum. The desired level of detail of both kinetic and transport phenomena models depend largely on the purpose of the model and a wide range is available in the literature.

The kinetic models can generally be labeled as either global or detailed. The detailed kinetic models do not only describe the reaction rate as a function of temperature and gas phase concentrations but at least one surface species coverage is also included. A number of these kinds of models for the DOC have been investigated with a large span in the numbers of modeled reactions and species, e.g. [1–3]. In global kinetic models the surface species have been eliminated from the reaction rates and instead inhibition terms are used. This simplification is based on an assumption of a rate limiting step [4] and will make the models more robust and computationally less demanding. Many of the successful global kinetic models for DOC [5–8] are based on the classical work of Voltz [9] performed in the 70s. Historically the global kinetic models have been the preferred type for describing DOC kinetics but for simulation of transients the

* Corresponding author.
E-mail address: derek.creaser@chalmers.se (D. Creaser).

http://dx.doi.org/10.1016/j.apcatb.2016.03.024
0926-3373/

Nomenclature

Roman symbols Description (Units)

A	Mass transfer area (m^2)
A	Preexponential factor (mol (kg Pt)$^{-1}$ s^{-1} or m^3 (kg Pt)$^{-1}$ s^{-1})
C	Concentration (mol m^{-3})
d	Channel diameter (m)
d_p	Pore diameter (m)
D	Bulk gas diffusivity (m^2 s^{-1})
$Deff$	Effective diffusivity (m^2 s^{-1})
DK	Knudsen diffusivity (m^2 s^{-1})
Ea	Activation energy (J mol^{-1})
f_D	Ratio of void fraction and tortuosity (–)
F_{tot}	Molar flow rate (mol s^{-1})
ΔH_{net}	Enthalpy change for NO oxidation reaction (J mol^{-1})
k	Rate constant (mol (kg Pt)$^{-1}$ s^{-1} or m^3 (kg Pt)$^{-1}$ s^{-1})
kc	Mass transport coefficient (m s^{-1})
m_{Pt}	Mass of Pt in washcoat segment (kg)
M	Molecular weight (kg mol^{-1})
N_s	Sites in washcoat segment (mol)
P	Total pressure (Pa)
r	Reaction rate (mol (kg Pt)$^{-1}$ s^{-1})
res	Residual (–)
Re	Reynolds number (–)
Sc	Schmidt number (–)
Sh_∞	Asymptotic Sherwood number (–)
ΔS_{net}	Entropy change for NO oxidation reaction (–)
t	Time (s)
T	Temperature (K)
w	Weighting factor (–)
X	Mean fractional conversion (–)
y	Molar fraction (–)
Δz	Length of segmental tanks (m)

Greek symbols

β	Adsorbed species index (–)
Γ	Lumped mass transfer coefficient (m^3 s^{-1})
θ	Fractional surface coverage (–)
ν	Stoichiometric coefficient of gas phase species (–)
χ	Stoichiometric coefficient of adsorbed species (–)

Subscripts

i	Gas component index
j	Reaction index
k	Tank index
n	Layer index

inclusion of surface species may be needed to obtain a satisfactory compromise between model accuracy and computational demands [3]. Inhibition terms for hydrocarbons and CO in global kinetic rate expressions account for competitive adsorption of these species on sites. However, it has also been found that hydrocarbons can have an apparent inhibition effect on NO oxidation resulting from NO_2 acting as an oxidant in the reaction with hydrocarbons [10]. In addition it has been reported that for simulation of DOC performance under actual vehicle operating conditions, these common global kinetic models lack such reactions to account for an observed negative efficiency behavior of NO oxidation at low exhaust gas temperatures [11].

Two types of heat and mass transfer are of high importance for the catalyst model. Firstly the external transport from the gas bulk to the washcoat surface and secondly the internal transport inside the washcoat itself. The external transport is often modeled with a film model using flow properties, geometry and a gradient between the gas bulk and the washcoat surface to determine the transport rate. Several models for external heat and mass transfer parameters have been developed for catalytic monolith converters [12–14]. The internal mass transfer of different components is usually described by the effective diffusivity which is a function of the structure of the washcoat, gas composition and temperature. Effective diffusivity may either be measured by for example chromatographic [15] techniques or with a Wicke Kallenbach diffusion cell [16], or it may be calculated from models requiring detailed knowledge of the washcoat pore structure [17–19]. Regardless if the effective diffusivity is calculated or measured, specialized equipment and measurements are needed in addition to the experimental setup used for the kinetic experiments.

The conversion in a monolith catalytic converter can be either reaction rate limited or mass transport limited depending on inlet conditions and catalyst configurations such as noble metal loading and washcoat thickness [20]. If kinetic parameter estimation is to be performed mass transport limited conditions should either be carefully avoided or the catalyst model must be able to give a good description of both external and internal mass transport. Otherwise the kinetic parameters may be influenced by transport limitations and thereby not intrinsic. Internal mass transfer limitations have been shown to be of importance for operation of SCR [21–23], NO_X storage catalysts [22], ammonia slip catalysts [24] and dual layer catalysts [25,26] but for DOC the area is less studied. To highlight the effect of internal transport limitations, studies have also been made where an extra layer of inert washcoat layer was placed on top of the active washcoat layer [18].

The current study aims to develop a kinetic and transport model for DOCs with a satisfactory compromise between accuracy, computational demands and robustness for simulation of transient full-scale operation. Specifically the model shall account for surface concentrations of key species needed to capture transient kinetic features for typical lean exhaust engine conditions. The need for reactions in the kinetic model accounting for apparent inhibition effects of hydrocarbons and CO due to their reactions with NO_2 will be investigated. In addition, the model should properly account for transport limitations and distinguish them from reaction kinetics. To achieve this, lab scale experiments were performed with DOCs with different platinum loadings and three different washcoat configurations of which two had an inert top layer. Both kinetic parameters for a detailed kinetic model and effective diffusivities will be optimized for the experimental data using a single channel catalyst model.

2. Modeling method

This section includes a description of the reactor model, an of outline the adjustable parameters and the definition of the objective function of the parameter estimation algorithm.

2.1. Reactor model

Transient experiments have been shown to be significantly more rich in information than experiments at steady state [27]. The experiments in this study will therefore be of transient nature which also means that the reactor model used will need to be able to describe the dynamic behavior of a monolith catalyst reactor. In the present model the accumulation of surface species will serve to capture this dynamic phenomenon. A single channel model previously presented by the authors [28] was used. The monolith channel was discretized as tanks in series where the catalyst washcoat was discretized both radially (as layers) and axially while the gas phase was only discretized axially, see Fig. 1. This 1D/2D (gas

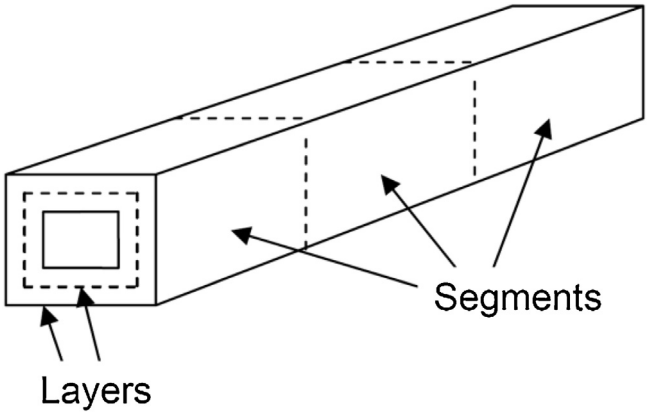

Fig. 1. Illustration of the catalyst discretization principle demonstrated by a single channel.

phase/washcoat) structure was chosen since it was considered a good compromise between accuracy and computational speed [29]. The gas phase mass balance in each tank was described by a static balance between axial convective flow and transport to the catalyst washcoat. Similarly, the mass balance in each washcoat layer was described by diffusion and reactions. The mass balances in the gas phase (n = 0) and washcoat layer (n ≥ 1) are described by Eqs. (1) and (2), respectively.

$$F_{tot}\left(y_{i,k-1,0}-y_{i,k,0}\right)-\Gamma_{i,k,0}\left(C_{i,k,0}-C_{i,k,1}\right)=0 \quad (1)$$

$$\Gamma_{i,k,n-1}\left(C_{i,k,n-1}-C_{i,k,n}\right)-\Gamma_{i,k,n}\left(C_{i,k,n}-C_{i,k,n+1}\right)+\sum_{j}\nu_{i,j}r_{j,k,n}m_{Pt,k,n}=0 \quad (2)$$

The lumped mass transfer coefficients $\Gamma_{i,k,n}$ are:

$$\Gamma_{i,k,0}=\frac{A_k}{\frac{1}{kc_{i,k}}+\frac{0.5\cdot\Delta X_1}{D_{eff,i,k}}} \quad (3)$$

$$\Gamma_{i,k,n}=\frac{A_k}{\frac{0.5\cdot\Delta X_n}{D_{eff,i,k}}+\frac{0.5\cdot\Delta X_{n+1}}{D_{eff,i,k}}} \quad (4)$$

for $n=1\ldots N-1$ and for $n=N$, $\Gamma_{i,k,N}=0$.

Accumulation terms in the mass balances (Eqs. (1) and (2)) were neglected because the characteristic time constants for these transport processes are small compared to accumulation of species on the catalyst surface. The dynamic mass balance of surface species is given by:

$$N_{s,k,n}\times\frac{d\theta_{\beta,k,n}}{dt}=\sum_{j}r_{j,k,n}\chi_{\beta,j}m_{Pt,k,n} \quad (5)$$

The lab reactor used in the study was designed to minimize heat losses to the environment by heating the outer catalyst wall with the gas flow before it enters the catalyst (Fig. 2). An adiabatic heat balance was used as described earlier [28], however for the experimental conditions used here with low concentrations of reactants, high space velocities and moderate temperature ramp rates the reactor was predicted to operate isothermally under all conditions.

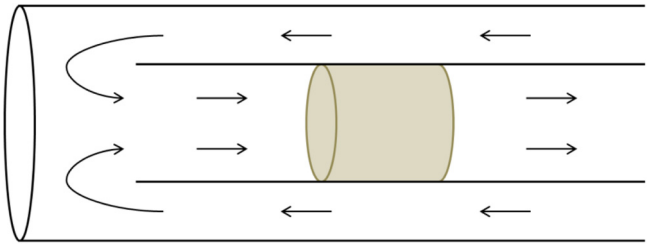

Fig. 2. Illustration of the lab rig heating principle. Note that the incoming flow surrounds the monolith.

2.1.1. Mass transfer

The external mass transfer resistance was described by a film model for square channels with laminar flow introduced by Hawthorn [30]:

$$kc_{i,k}=\frac{Sh_\infty\times D_{i,k}}{d}\times\left(1+\frac{0.095\times Re\times Sc\times d}{\sum_{z=1}^{k}\Delta z_z-0.5\times\Delta z_k}\right)^{0.45} \quad (6)$$

The asymptotic Sherwood number (Sh_∞) was set to 3. The principle for heat and mass transfer in the washcoat is described in the previous work by the authors [28]. In the current study the washcoat included in some cases an inert layer. The inert washcoat was radially discretized as two tanks in series (in addition to the eight that described the active washcoat layer) where the first tank was only 0.5% of the inert washcoat thickness. The motivation for only using two extra layers is based on the fact that no reaction will take place in the inert washcoat and thus the concentration gradient can be assumed to be linear. Initial values for the pore diffusion effective diffusivity were estimated based on an additive resistance, also known as the Bosanquet formula:

$$D_{eff,i,k}=\frac{f_D}{\frac{1}{D_{i,k}}+\frac{1}{DK_{i,k}}} \quad (7)$$

where f_D is a factor that takes into consideration the porosity and tortuosity of the porous material. $DK_{i,k}$ is the Knudsen diffusivity which was calculated from:

$$DK_{i,k}=\frac{d_p}{3}\sqrt{\frac{8RT_{s,k}}{\pi M_i}} \quad (8)$$

2.2. Adjustable parameters

To tune the model to the measurement data a number of parameters in scaled and centered forms [31] were adjusted. These parameters can be divided into kinetic parameters and mass transfer parameters.

In a previous study [28] scaling the effective diffusivities were evaluated as a method of tuning the transport resistance with the aim of reducing the correlation between mass transport and kinetic parameters. The species were divided into two groups, where the first group contained O_2, NO, NO_2, and CO and the second group contained C_3H_6. In the first group all species are small molecules with similar diffusivities and could be expected to have similar mass transport properties in the washcoat with presumably the same bias from their true values. To reduce the number of parameters to tune, the effective diffusivities for all these components were adjusted with the same factor. The factor was denoted as the effective diffusivity scaling factor for small molecules ($f_{Dscl,S}$) and was simply an amplification of the effective diffusivity values for all these molecules. Even though the second group of molecules only contains propene, and not a wide range of unknown hydrocarbons as in the previous study, the properties of propene was still considered different enough to motivate its own effective diffusivity scale factor ($f_{Dscl,L}$). The effective diffusivity scaling factor for small molecules was tuned to adjust mass transport resistance for all reacting species except propene whose transport resistance will be adjusted with its specific effective diffusivity scaling. Two mass transport parameters were thereby tuned to the experimental data together with the kinetic parameters introduced below.Tuning both the forward and backward reaction rates in an equilibrium reaction would result in very high correlation between the kinetic parameters. The high correlation would complicate the parameter estimation and most likely make the process of finding a good

fit to measurement data slower. For reversible reaction steps only the kinetic parameters of the desorption reaction were therefore estimated in the current study. This reduces not only the correlation between parameters but also parameter estimation time since the number of parameters to estimate is lower. The structure of the kinetic model is one outcome of this study, and thus a further description of the tuned kinetic parameters will be given in the Section 4.

2.3. Parameter estimation method

The method used for parameter estimation in the current study is the gradient search method that has proved successful in numerous fields and applications [32]. This means that the definition of the residuals as well as the selection and scaling of the parameters will be of greatest importance for the parameter estimation. Selection of parameters to estimate has already been discussed in Section 2.2 and the scaling has been described in a previous study by the authors [28], but the residual calculation needs further description which will be given directly below.

2.3.1. Residual calculation

In a previous study [33] it was found that a more even influence from the components was achieved if conversions were used instead of concentrations when calculating the residuals. To achieve this, the residuals were calculated according to Eq. (9).

$$res_i = \left[\frac{y_{i,in} - \hat{y}_{i,out}}{y_{i,in}} - \frac{y_{i,in} - y_{i,out}}{y_{i,in}}\right] * w = -\frac{\hat{y}_{i,out} - y_{i,out}}{y_{i,in}} * w_i \quad (9)$$

where w_i is a weighting factor (further described below), $\hat{y}_{i,out}$ is the simulated outlet mole fraction, $y_{i,out}$ is the measured outlet mole fraction and $y_{i,in}$ is the measured inlet mole fraction. To compensate for the fact that the NO oxidation conversion is limited by thermodynamic constraints the residual for NO was instead calculated relative to the equilibrium conversion possible at the current condition as shown in Eq. (10).

$$res_{NO} = \left[\frac{\left(y_{NO,in} - y_{NO,out,lim}\right) - \left(\hat{y}_{NO,out} - y_{NO,out,lim}\right)}{y_{NO,in} - y_{NO,out,lim}} - \frac{\left(y_{NO,in} - y_{NO,out,lim}\right) - \left(y_{NO,out} - y_{NO,out,lim}\right)}{y_{NO,in} - y_{NO,out,lim}}\right] * w_{NO}$$

$$= -\frac{\hat{y}_{NO,out} - y_{NO,out}}{y_{NO,in} - y_{NO,out,lim}} w_{NO} \quad (10)$$

here $y_{NO,out,lim}$ is the lowest molar fraction of NO possible via NO oxidation at the inlet conditions due to thermodynamic constraints. Since NO_x reduction was negligible at the lean exhaust experimental conditions used here, the fit for NO_x was considered to be described well enough by only the NO residual. In addition to NO, the residuals of both C_3H_6 and CO were used for parameter estimation.

The weighting factor w_i is calculated according to Eq. (11).

$$w_i = \frac{1}{X_i\sqrt{n_i}} \quad (11)$$

where n_i is the number of data points used for residual calculation for species i and X_i is the mean absolute fractional conversion in the n_i data points for component i. On a concentration level the NO oxidation conversion is higher than for the other components, but since the inlet concentration is very high the fractional NO oxidation conversion will still be low. The conversion dependent weighting factors are therefore used to balance the influence on the residual for components with different levels of conversion.

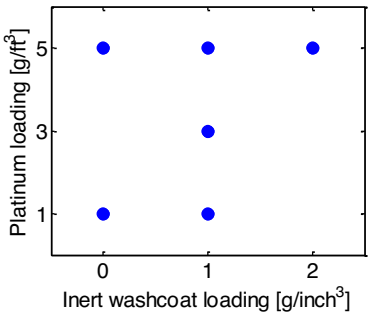

Fig. 3. Schematic description of catalyst configurations.

For data sets with very low fractional and concentration conversion the weighting could mean that too much focus is put on fitting concentrations where the conversion is a result of measurement uncertainties. It is therefore important to carefully evaluate the properties of data before the weighting is applied.

3. Experimental method

The aim of this section is to describe the experimental conditions for the study starting with the reactor and catalyst samples and concluding with the performed experiments

3.1. Laboratory reactor

The experimental data used for model development was measured in a laboratory scale reactor. The inlet gas composition was controlled by mass flow controllers and the gas mixture temperature was controlled by an oven that also contained the monolith itself. The flow through the oven was heat exchanged with the monolith in a recirculating design according to Fig. 2. This design was chosen to achieve a more even temperature distribution in the monolith compared to what would be possible if the monolith would be heated only by the incoming flow.

Gas temperature was measured with 1.5 mm thermocouples positioned at the center of the pipe close to the catalyst outlet. The gas phase concentrations were measured after the catalyst with separate analyzer units. The concentration of CO was measured with infrared spectroscopy, NO and NO_2 were measured with chemiluminescence, total hydrocarbons were measured with flame ionization and O_2 was measured with an electrochemical cell.

The gas composition entering the catalyst was adjusted to the correct inlet conditions at low temperature before the heating ramp was applied; the inlet concentrations in the presented results are therefore set equal to the set-points of the gas flow controller. The total gas flow rate was 20 L/min for all experiments.

3.2. Catalysts

To obtain a wide span of experimental data, six different catalyst configurations with different platinum loadings and inert washcoat layer thicknesses were used. All catalysts, shown in Table 1, had an active washcoat loading of 1 g/inch^3, a monolith length and diameter of 1 inch and cell density of 400 cpsi. The same washcoat material was used for both the inert and the active washcoat layer even though the latter, of course, also contained platinum. The platinum loadings were 1, 3 and 5 g/ft^3. These relatively low loadings were chosen to avoid complete conversion of reactants or thermodynamic control which was noted to be problematic in our previous study [28].The catalysts were platinum only model catalysts provided by Johnson Matthey.

Table 1
Catalyst configuration used for parameter estimation.

ID#	Pt loading [g/ft^3]	Inert washcoat loading [g/inch^3]	Average inert wash-coat thickness [μm]	Average total washcoat thickness [μm]
1	1	0	0	35
2	5	0	0	35
3	1	1	37	72
4	3	1	37	72
5	5	1	37	72
6	5	2	78	113

A visual display of the catalyst configurations are given in Fig. 3. The reason for only including one catalyst configuration with the highest inert washcoat loading was that conversions were expected to be very low for the selected experimental range for the lower platinum loadings of 1 g/ft^3 and 3 g/ft^3.

3.3. Experiment conditions

To achieve good conditions for parameter estimation it is important to have experimental conditions that span the data range, where the model is aimed to be applied, as effectively as possible. In the current study the desired model application is for the simulation of full scale systems with heavy duty diesel engines under lean operation (excluding active regeneration of the DPF) which means that the catalyst inlet temperature and concentrations should be in the range of what such an engine may produce. The experiments should include both a complete synthetic exhaust gas mixture as well as simpler ones that enable estimation of parameters where the reactions take place with or without competition between the different oxidation reactions. It is also important that conversions of the components also cover a wide span. To achieve these desired properties of the data four different experiments were performed on every catalyst configuration. The inlet concentrations for these experiments were kept constant at the levels given in Table 2. These concentration levels were selected to mimic those in the exhaust from a Euro IV calibrated heavy duty diesel engine [28].

In addition to the components in Table 2 all gas mixtures also contained 5% CO_2, 5% H_2O, 14% O_2 and balance N_2. For all experiments a low initial temperature was chosen to avoid reaction at the starting point of the experiments. The temperature was ramped from the low initial temperature up to a maximum temperature where the conversion was expected to be high and then ramped down to the initial temperature again. The temperature levels and ramp rates are also summarized in Table 2.

For the light-off experiments the inlet temperatures were increased from the minimum temperature to the maximum temperature at a high rate. The temperature was subsequently decreased at a similar rate back to the initial temperature after the maximum temperature had been held constant for about five minutes. The average temperature ramp rate for these experiments was between 10 and 25 °C/minute depending on the experimental type, see Table 2. The higher ramp rate was achieved for the NO oxidation light-off experiments where the difference between initial and maximum temperature was largest. The temperature changes for the complete gas mix experiments were performed stepwise with 50 °C intervals with the intention to achieve near steady-state conditions at every temperature level. Each temperature level was maintained for 10 min.

Three fresh samples of catalyst 1 and of catalyst 2 were each used for dispersion measurements. X-ray fluorescence (XRF) was used to measure the platinum loadings for the six samples and CO chemisorption was used to determine the dispersions. The average dispersion was 35.8% for samples of catalyst 1 and 32.3% for samples of catalyst 2. Due to the very low CO uptake observed from samples from catalyst 1, the dispersion measurement may contain a significant amount of experimental error. The measurements from catalyst 2 are more reliable and since the difference between the results is well within the margin of error for catalyst 1 the results from catalyst 2 were assumed to apply for both catalysts. The additional inert washcoat layer was considered to have no effect on the dispersion and the results for catalyst 2 were therefore applied in the modeling of catalyst 3, 4, 5 and 6 as well. An analysis based on NO oxidation activity data from the lab rig could further verify a near equal dispersion independent of Pt loading. These results are further discussed in the last part of Section 4.1.

4. Results and discussion

In the current section the experimental evidence and development of the kinetic model structure is first reviewed before the final parameter estimated model is presented and its performance analyzed.

4.1. Analysis of experimental results

The first topic for discussion is hysteresis effects in light-off experiments. It is well known that when the inlet gas temperature is slowly increased and then decreased the conversion for a certain component may display strong hysteresis behavior. This means that the temperature where the conversion for the component starts to increase rapidly during heating (ignition) may not be the same temperature as the temperature where the conversion starts to decrease (extinction). The phenomena can have a physical explanation such as accumulation of heat in the substrate and washcoat but from a kinetic point of view the hysteresis is generally a result of the dynamic behavior of the catalyst surface species and reactions. Varying conditions on the catalyst surface can mean that the catalyst surface coverage at low temperature is dominated by a single component inhibiting the adsorption of other reacting components. This is known as an inhibition effect and results in a hysteresis where the ignition temperature is higher than the extinction temperature. This hysteresis is typical for the CO oxidation and has been well documented in different studies for example by Salomons et al. [3]. For NO oxidation a hysteresis with opposite dynamics, called inverse hysteresis, has been identified and shown to be a result of Platinum oxide being formed on the surface at high temperature giving a higher extinction temperature than ignition temperature [34–36].

In the discussion of hysteresis phenomena the results from light-off experiments performed on catalyst 4 will be used since this is the catalyst found in the center of the experimental plan (see Fig. 3) and thereby should be fairly representative for all catalysts used in the study. In Fig. 4 the CO light-off experiment, described in the previous section, for catalyst 4 is shown. Both panel a and b of Fig. 4 show that the experiment had a clear hysteresis and if panel b is studied it is evident that the temperature difference between extinction and ignition is about 50 °C.

If the light-off experiment for the same catalyst but for NO oxidation is studied, seen in Fig. 5, the trend is not as clear as it was for CO. One complicating factor is the thermodynamic equilibrium of the NO oxidation reaction which makes the NO_{out} graph less uniform since the conversion of NO reaches equilibrium at the highest tem-

Table 2
Experimental Conditions.

Experiment Type	Inlet concentrations				Temperature levels and ramp rates		
	NO [ppm]	NO_2 [ppm]	C_3H_6 [ppm]	CO [ppm]	Initial [°C]	Maximum [°C]	Temp. ramp rate [°C/min]
CO light-off	–	–	–	100	60	360	10
C_3H_6 light off	–	–	50	–	80	360	10
NO oxidation light-off	800	–	–	–	100	550	25
Complete gas mix	800	80	50	100	70	270	50[a]

[a] Stepwise changes with 50 °C intervals.

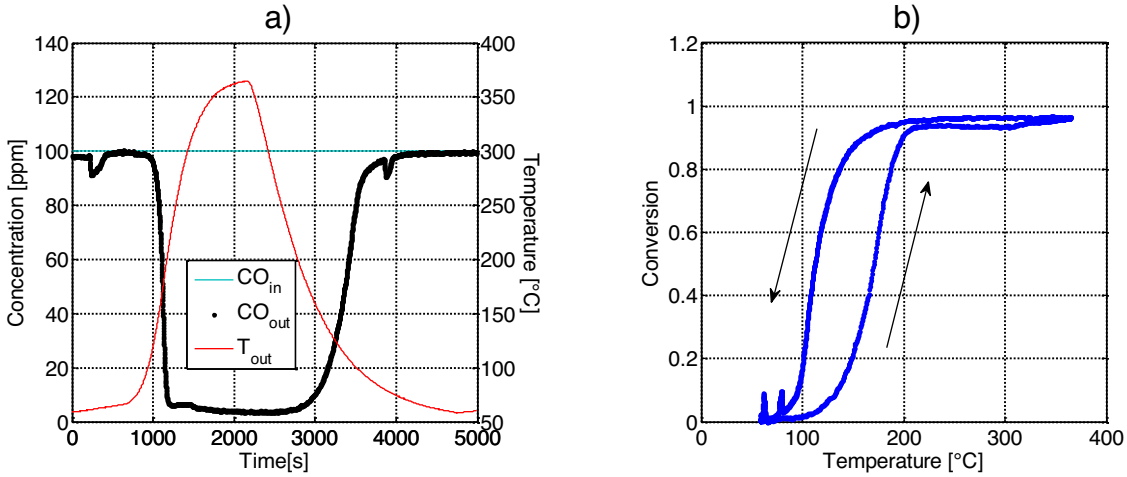

Fig. 4. CO light-off for catalyst 4; a) concentration CO and temperature, b) CO conversion.

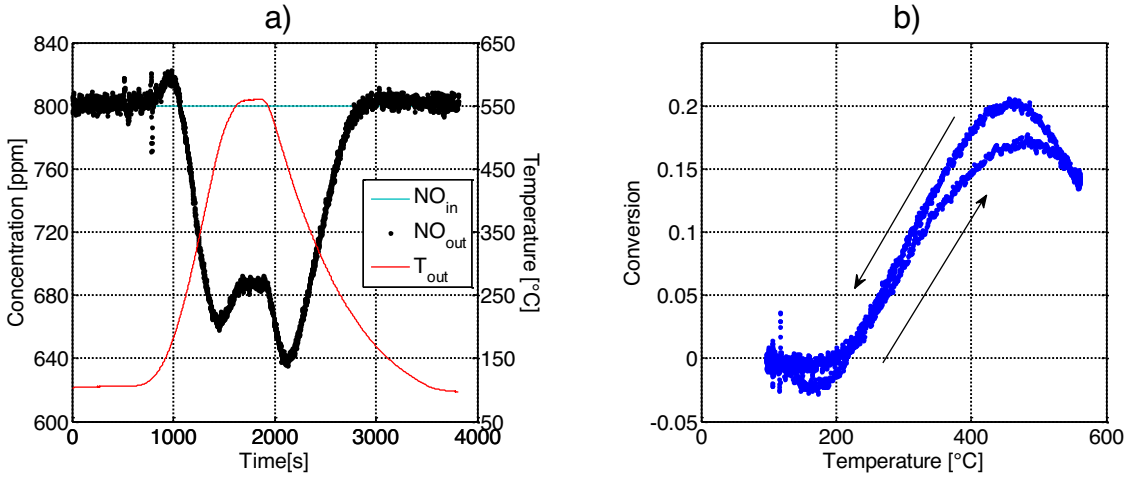

Fig. 5. NO oxidation light-off for catalyst 4; a) concentration NO and temperature, b) NO oxidation conversion.

peratures. Panel a of Fig. 5 clearly shows a higher conversion when the temperature is decreasing than when it is increasing, which is the opposite behavior of what is typically observed and ascribed to formation of platinum oxide. A similar behavior was found in a study by Watling et al. [37] where the hysteresis was attributed to increased platinum-oxide coverage at the start of the experiment as a result of catalyst pre-treatment. It has been shown that platinum oxide formation is maximized in a temperature window of about 250–300 °C [36,38]. At low temperature platinum oxide can be reduced by NO, while at higher temperatures it starts to decompose. Considering the fact that no specific pre-treatment was used in the current study, it is possible that the catalyst was initially partly covered with platinum oxide that further accumulated to some extent during the first part of the heat-up period. When the temperature dwelled for some minutes at the maximum of 550 °C, a part of the platinum oxide decomposed to its metallic state, resulting in higher activity for NO oxidation during the first part of the cool-down period. However, when reaching 300 °C, the platinum oxide formation prevailed again to give a similar activity as during the heat-up period. However, it cannot be ruled out here that at least part of the source of the hysteresis in this case is linked to the temperature ramp itself. The temperature ramp rate for the NO oxidation light-off experiments were particularly fast and this could have led to some temperature gradients in the monolith resulting in lower reaction rates when the monolith is heated up compared to when it is cooled down, even though the measured outlet temperature is the same. Regardless, without any pre-treatment of the catalyst to control the oxidation state of Pt, the experiments

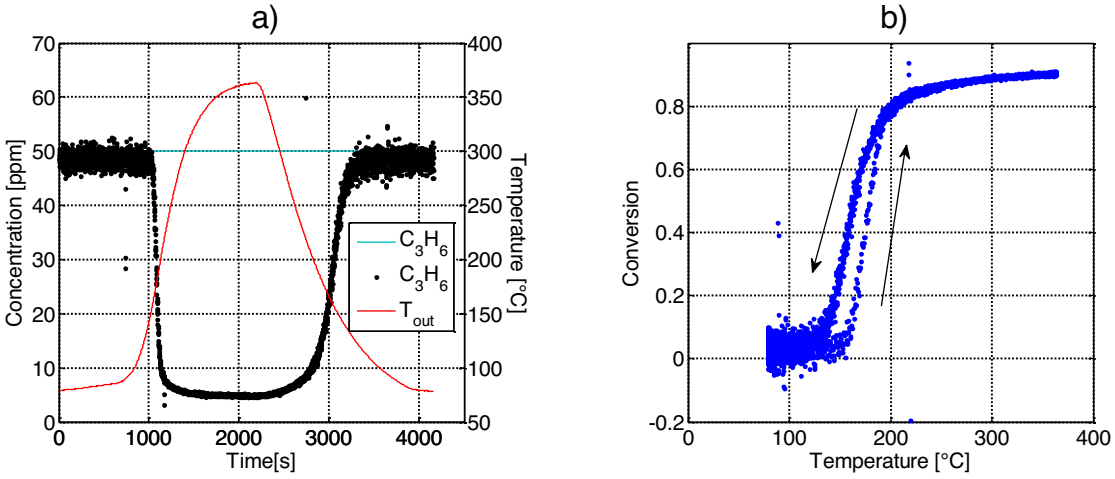

Fig. 6. C_3H_6 light-off for catalyst 4; a) concentration C_3H_6 and temperature, b) C_3H_6 conversion.

are unsuitable for modeling platinum oxide formation. Although modeling results will be shown for both the heating and cooling periods below, the cooling periods are most relevant since it can be assumed that all samples begin following the heat up period with approximately the same state for Pt.

The light-off experiment for C_3H_6, shown in Fig. 6, shows some hysteresis but not as emphasized as for CO. The difference between the extinction point and the ignition point is less than 20 °C and, as for NO, this may be partially connected to the thermal dynamics of the experiment than the properties of the catalyst surface.

An important feature of the experiments was that they should provide data that makes it possible to differentiate between mass transport and kinetics. If the platinum dispersion of catalysts 2, 5 and 6 are assumed to be equal all the differences in the results of experiments with these catalysts should be a function of the different inert washcoat thicknesses. The CO light-off experiments for these three catalysts are compared in Fig. 7 (panel b and c) which shows a noticeable difference in conversions. The catalyst with no inert layer (catalyst 2) reaches 100% conversion for a large part of the experiment even though the maximum temperature was about 15 °C lower than for the experiment with the other catalysts. The catalyst with the thickest washcoat layer (catalyst 6) reaches the lowest maximum conversion and neither of the two catalysts with an inert layer reaches 100% conversion. The rate of the extinction clearly decreases with increased inert washcoat thickness which even generates a higher conversion for catalyst 6 than for the other two catalysts at about 4000 s. However, an increased inert washcoat layer does not appear to have a large influence on the ignition behavior.

The results in Fig. 7 clearly show the effects of transport resistance and they are even more pronounced for the corresponding C_3H_6 light-off experiments shown in Fig. 8 (panel b and c). Again the catalyst with the thickest washcoat layer reaches the lowest maximum conversion. These results are expected since propene has a lower diffusivity than CO. For the NO oxidation light-off only the experiments with catalyst 5 and 6 are analyzed since the temperature of the experiment on catalyst 2 was too divergent to make a feasible comparison. For completeness all three sets of experimental data are, however, shown in panel b and c of Fig. 9. Between 1000 and 1500 s there is a noticeable difference between catalyst 5 and 6, but there is also an offset in concentrations at the beginning of the interval and prior to the temperature ramp which makes the difference more pronounced. This offset is likely a product of experimental error since the measured NO outlet concentration from catalyst 6 is clearly above the inlet set-point of 800 ppm at

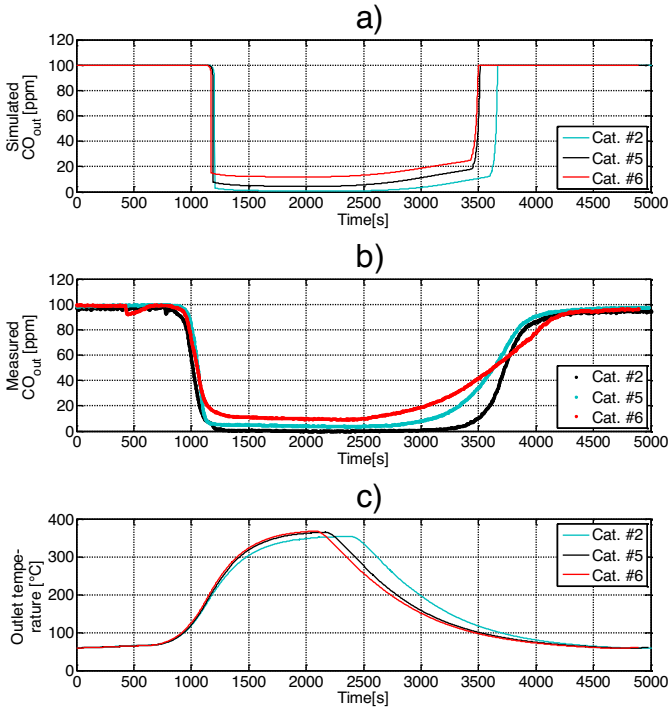

Fig. 7. CO light-off for catalysts 2, 5 and 6 with 5 g/ft^3 platinum loading but with different inert washcoat loadings (0, 1 and 2 g/inch^3 respectively); a) simulated outlet concentration of CO, b) measured outlet concentration of CO, c) measured outlet temperature.

1000 s. Between 1500 and 2000 s thermodynamic equilibrium is reached for both catalysts where the about 5 °C higher temperature for catalyst 6 gives a lower conversion. After 2000 s the difference in conversion is low except for around 2200 s in the area where the effect of thermodynamic limitations starts to decrease. To summarize the effect of transport limitations in the NO oxidation light-off experiments are less obvious than for the CO and C_3H_6 light-off experiments. This may be a result of less experimental time spent at temperatures between kinetic and thermodynamic controlled regimes but could also result from the NO oxidation reaction rate simply being generally lower than that for CO and C_3H_6 oxidation and therefore not entering a regime with as severe mass transport limitation for the current experimental conditions. That diffusion of NO being less hindered by added washcoat thickness is also a

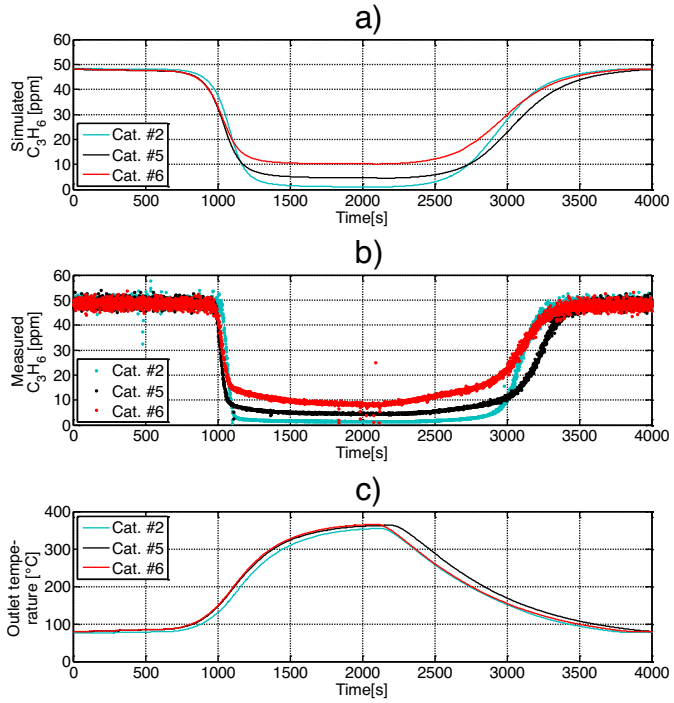

Fig. 8. C_3H_6 light-off for catalysts 2, 5 and 6 with 5 g/ft^3 platinum loading but with different inert washcoat loadings (0, 1 and 2 g/inch^3 respectively); a) simulated outlet concentration of C_3H_6, b) measured outlet concentration of C_3H_6, c) measured outlet temperature.

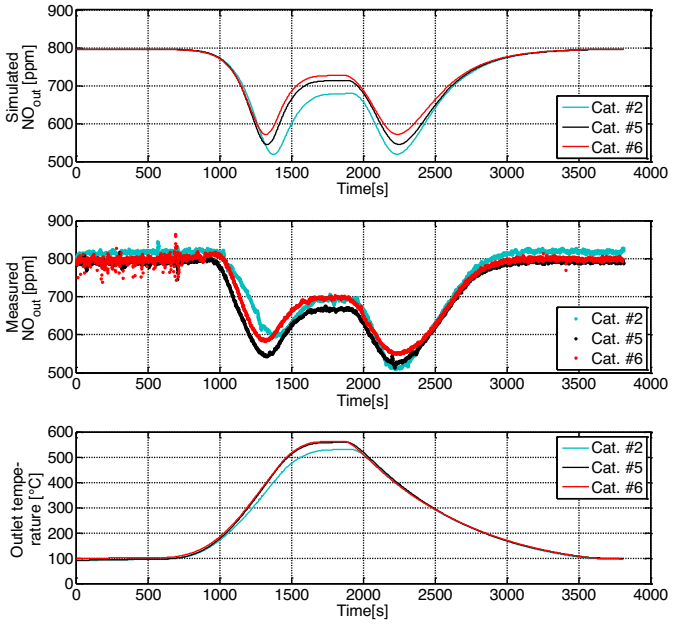

Fig. 9. NO oxidation light-off for catalysts 2, 5 and 6 with 5 g/ft^3 platinum loading but with different inert washcoat loadings (0, 1 and 2 g/inch^3 respectively); a) simulated outlet concentration of NO, b) measured outlet concentration of NO, c) measured outlet temperature.

possible explanation but due to the similarity between NO and CO it is less likely. From the above discussion it can be concluded that light-off experiments with CO, C_3H_6, and NO were influenced by the introduction of different thicknesses of inert washcoat layers and that mass transport resistance did limit the conversions. However the limitations were not as pronounced for NO as for C_3H_6 and CO.

Fig. 10 shows the results of the complete gas mix experiment performed on catalyst 4. The first observation is that the CO oxidation starts at about 60 °C which is significantly lower than what was measured for the light-off experiments shown in Fig. 4. C_3H_6 on the other hand appears to have a 10–20 °C later ignition than in the C_3H_6 light-off experiment shown in Fig. 6. The outlet concentration of NO is higher than the inlet concentration for the majority of the experiment at the same time as NO_2 is below its inlet concentration. NO is thereby oxidized to form NO_2 at a lower rate than NO is produced from NO_2. The fact that the oxidation of CO coincides very well with the partial reduction of NO_2 during the first 4000 s of the experiment indicates that NO_2 could have reacted with CO causing formation of NO and CO_2. Between 4000 and 8000 s the NO formation does not increase which is likely a result of CO being oxidized by both O_2 and NO_2 at these temperatures. The delay in C_3H_6 ignition compared to the light-off experiment could be a result of an increased number of surface components reducing the oxygen coverage or simply increased competition with other species for reaction sites. These results are similar to those reported earlier in the literature, where it was observed that NO_2 reacted with various hydrocarbons including propene to form NO and thus cause an apparent inhibition of NO oxidation [10]. However, in this earlier study gas mixtures were used that contained only hydrocarbons and no CO. It is however evident here that for a complete synthetic exhaust gas mixture, NO_2 reacts preferentially with CO rather than the hydrocarbon, in this case propene.

Since the uncertainty of the dispersion measurements was high particularly for samples with the lowest Pt loading, a simple validation was made based on the experimental data. This involved a comparison of the average conversion for three catalysts with different Pt loading but with equal inert washcoat thickness. To achieve useful results it is important that the data used is free of mass transport limitations and that the conversion is below the equilibrium maximum conversion in the studied temperature interval. As a consequence the validation was made on NO oxidation light-off experiments for catalysts 3, 4 and 5 in the temperature interval 410–440 °C. As previously discussed the NO oxidation light-off experiments displayed a hysteresis giving higher conversion after the maximum temperature was reached than before. Data points were therefore only taken from the later parts of the experiments in the dispersion analysis. The chosen data set had the lowest possible maximum conversion of 36% for catalyst 5 with highest Pt loading, yet a very low but measurable conversion for catalyst 3 with the lowest loading. In addition there was sufficient margins from thermodynamic limits (>70 ppm). The result of the analysis is shown in Fig. 11 where the calculated mean observed reaction rate is compared for the different catalysts over the given temperature intervals.

The trend line in Fig. 11 shows the expected observed reaction rate if the dispersion for catalyst 4 and 5 would be equal to the dispersion of catalyst 3 (1 g Pt/ft^3). The figure indicates that the dispersion does not differ significantly between the catalysts, confirming the experimental dispersion measurements by CO chemisorption. The results from the dispersion measurements on catalyst 2 were therefore used for modeling of all catalysts.

4.2. Development of kinetic model

The three main reactions of the DOC are the oxidations of CO, NO and hydrocarbons (HC) by oxygen. There are however several additional reactions that may be included in the reaction kinetics such as H_2 oxidation [39,40], CO oxidation by NO_2 [37] and NO_x reduction by HC [7,41–44]. The oxidation of HC can also be described in different levels of detail if a complex composition of HC, such as that from an engine, is to be modeled. For models where HC is represented by one molecular species, propene is the usual choice [9,11,45]. The

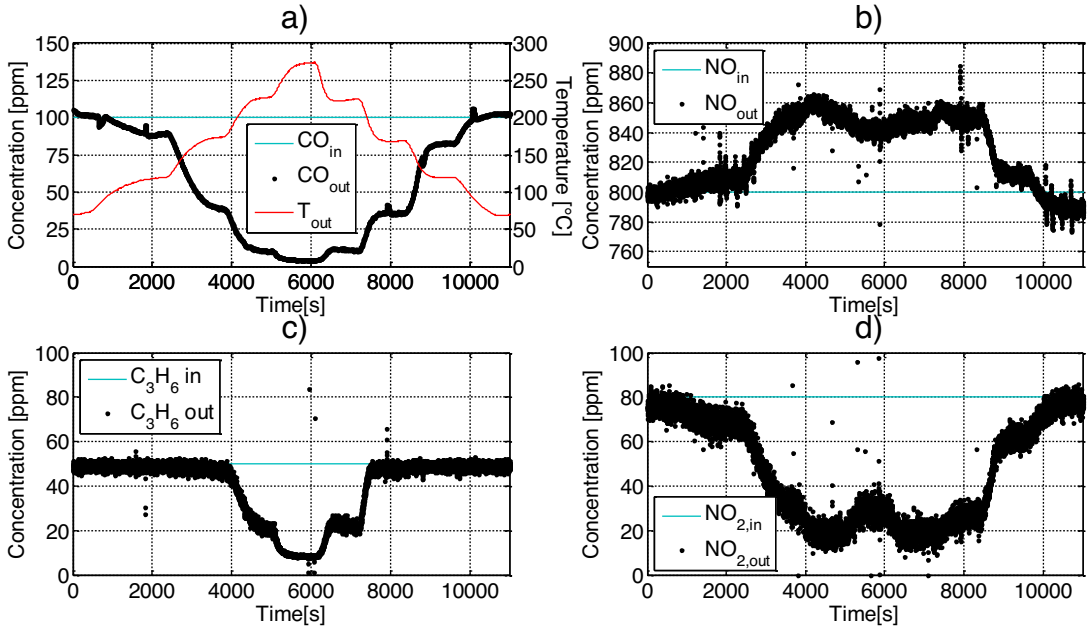

Fig. 10. Complete gas mix experiment for catalyst 4; a) CO concentration and temperature, outlet concentrations of b) NO, c) C_3H_6, and d) NO_2.

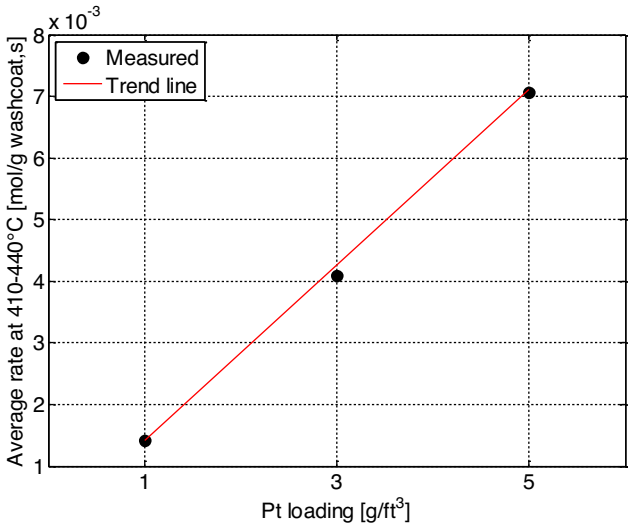

Fig. 11. Average observed reaction rate for NO oxidation light-off experiments for catalyst 3 (1 g Pt/ft^3), 4 (3 g Pt/ft^3), and 5 (5 g Pt/ft^3) between 410 and 440 °C.

current study was performed at lab scale which means that HC was represented by propene to agree with the majority of the kinetic models.

The literature offers a wide range of kinetic models of both detailed [46–50] and global type [51–53] that describe the NO oxidation over Pt-based catalysts. These models generally include adsorption of NO, NO_2 and O_2 but in what forms they adsorb on the sites and the pathways of reactions differ as well as the formulation of the kinetic expressions. In the current study NO oxidation was studied in parallel with CO and C_3H_6 oxidation, as well as mass transport and to reduce the complexity of the parameter estimation a simplified version of the detailed kinetic model for NO oxidation presented by Olsson et al. [46] was suggested according to Table 3 (reactions 1–6).

Compared to the model by Olsson et al. two simplifications were made. In the Olsson model gas phase NO is assumed to react directly with adsorbed O in an Eley-Rideal type of mechanism but the model

Table 3
Kinetic model.

#	Reaction	Rate
NO oxidation		
1	$O_2(g)+2^* \rightarrow 2O^*$	$r_1 = c_{O_2}\theta_v^2 k_1$
2	$2O^* \rightarrow O_2(g)+2^*$	$r_2 = \theta_O^2 k_2$
3	$NO_2(g)+^* \rightarrow NO_2{}^*$	$r_3 = c_{NO_2}\theta_v k_3$
4	$NO_2{}^* \rightarrow NO_2(g)+^*$	$r_4 = \theta_{NO_2} k_4$
5	$NO(g)+O^* \rightarrow NO_2{}^*$	$r_5 = c_{NO}\theta_O k_5$
6	$NO_2{}^* \rightarrow NO(g)+O^*$	$r_6 = \theta_{NO_2} k_6$
CO oxidation		
7	$CO(g)+^* \rightarrow CO^*$	$r_7 = c_{CO}\theta_v k_7$
8	$CO^* \rightarrow {}^*+CO(g)$	$r_8 = \theta_{CO} k_8$
9	$CO^*+O^* \rightarrow CO_2(g)+2^*$	$r_9 = \theta_{CO}\theta_O k_9$
10	$CO^*+NO_2{}^* \rightarrow NO(g)+CO_2(g)+^*$	$r_{10} = \theta_{CO}\theta_{NO_2} k_{10}$
C_3H_6 oxidation		
11	$C_3H_6(g)+9O^* \rightarrow 3CO_2(g)+3H_2O(g)+9^*$	$r_{11} = c_{C_3H_6}\theta_O k_{11}$
12	$C_3H_6(g)+9\,NO_2{}^* \rightarrow 9NO(g)+3CO_2(g)+3H_2O(g)+9^*$	$r_{12} = c_{C_3H_6}\theta_{NO_2} k_{12}$

still includes a NO adsorption reaction. This means that adsorbed NO only directly influences the NO desorption rate and thereby only has an inhibiting influence on the other reactions. In the analysis of the NO oxidation light-off experiments neither indications of NO inhibition, nor NO self-inhibition was possible to identify as the source of the hysteresis. To reduce the complexity of the model, the adsorption of NO and thereby NO surface coverage, was therefore neglected in the current kinetic model. This simplification was also used in the kinetic model presented by Mulla et al. [52] where NO surface coverage was neglected in the derivation of a global kinetic model. The model by Olsson et al. also includes a surface dependence of the activation energies of O_2 and NO_2 desorption that is sometimes excluded in other comparable models and was excluded in the current study as well. A NO_x balance over all experiments showed some areas where the outlet NO_x was below the inlet NO_x which could be an indication of NO_x reduction to N_2. Other parts of the data showed an increase in outlet NO_x in the same size range (about 5% at highest) which led to the conclusion that the NO_x reduction was not sufficiently evident for inclusion in the kinetic model since it could not be clearly distinguished from experimental uncertainties. As a result NO_x reduction is negligible for the engine exhaust conditions for which the experiments here

are intended to represent, however it should be noted that for other engine calibrations an exhaust may contain higher concentrations of HC and lower NOx that can result in significant NOx reduction in a DOC.

As shown in the previous section the CO light-off experiments show a clear hysteresis and CO adsorption should therefore be included in the kinetic model. The analysis of the complete gas mix experiments also showed that CO is oxidized by NO_2 at low temperatures which means that this reaction is also needed in the kinetic model. The kinetic model for CO oxidation is shown in Table 3 (reactions 7–10).

The light-off experiments with C_3H_6 showed clearly less hysteresis than CO which indicate that that phenomenon may not be a result of C_3H_6 inhibiting the reactive sites. Irani et al. [10] reported an inhibition effect of hydrocarbons on NO oxidation but stated that the effect mainly was a result of NO_2 being consumed by hydrocarbons. Khosravi et al. [43,44] performed experiments and modeling of reduction of NO by propene and recorded both formation of N_2 and N_2O during consumption of NO and propene. The studies were however performed at higher concentrations of hydrocarbons than in the current experiments and these reactions have been observed to depend to some extent on the type of hydrocarbon present [54,55]. From the complete gas mix experiments it is difficult to conclude if C_3H_6 is oxidized by O_2 and NO_2 or by O_2 alone. The fact that oxidation by NO_2 was observed at similar conditions [10] and that NO_2 showed strong oxidizing properties for CO are, however, strong arguments for including the reaction in the kinetic model. Since the adsorption of C_3H_6 was not apparent in the measurement data and had little documented effect at the current concentration levels (maximum 50 ppm) both C_3H_6 oxidation reactions are modeled as reactions with gas phase C_3H_6. The reaction mechanism and rate expressions for C_3H_6 oxidation in the kinetic model are also shown in Table 3 (reactions (11)–(12)).

All reaction rate coefficients, k_j, are described by Arrhenius expressions according to Eq. (12).

$$k_j = A_j e^{-\frac{E_{A,j}}{RT}} \tag{12}$$

The unit of the pre-exponential factor, A_j, depends on the reaction rate expression. Units for all reaction rates are mole/s, kgPt. The reaction rate for CO adsorption is the only reaction that also has a temperature dependent pre-exponential factor which gives a rate constant according to Eq. (13).

$$k_7 = A_7 T^{0.5} e^{-\frac{E_{A,7}}{RT}} \tag{13}$$

4.3. Modeling results

Half of the experimental data was used in the parameter estimation process and half of the data was used for verification, according to Table 4. The experiments used for parameter estimation were selected with the principle that the three different inert washcoat loadings should be represented for every experimental type. The data will then give good conditions for resolving kinetics from mass transport in all experiments.

After completing the parameter estimation the final parameter values of the tuned and the fixed parameters are displayed in Table 5. The fixed parameters for reaction 1 and 3 were taken from Olsson et al. [46] and the kinetic parameters for reaction 7 were taken from a study by Chatterjee et al. [56]. The parameters A_6 and $E_{A,6}$ were not directly tuned but were continuously changed to maintain the thermodynamic limitations of enthalpy (ΔH_{net}) and entropy change (ΔS_{net}) for the NO oxidation reaction. These adjustments were made according to Eqs. (14) and (15).

$$E_{A,6} = \frac{1}{2}\left(E_{A,1} - E_{A,2}\right) + \left(E_{A,4} - E_{A,3}\right) + \left(E_{A,6} - \Delta H_{net}\right) \tag{14}$$

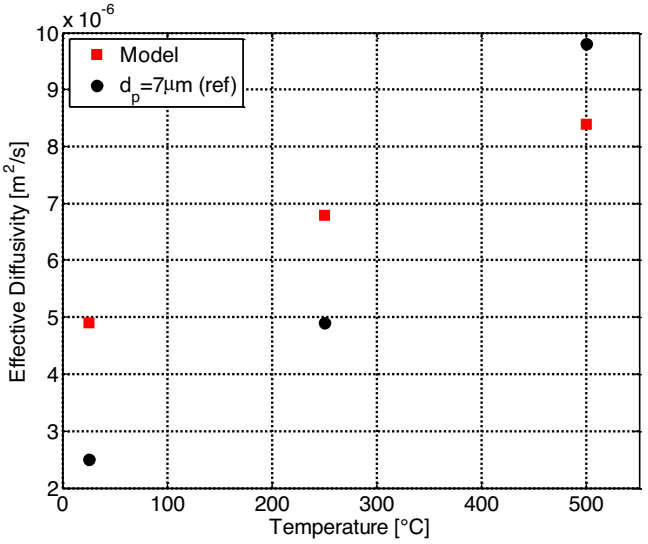

Fig. 12. Effective diffusivity for CO for the current model compared to the reference study [18].

$$A_6 = \left(\frac{A_1}{A_2}\frac{P}{RT_{ref}}\right)^{\frac{1}{2}} \frac{A_4}{A_3} A_5 exp\left(\frac{-\Delta S_{net}}{R}\right) \tag{15}$$

By studying the tuned parameters it can be concluded that the kinetic parameters for reaction 10, where adsorbed CO reacts with adsorbed NO_2, stand out compared to the others. The pre-exponential factor is very low but at the same time the activation energy is also low. This gives a reaction that will have less temperature dependence than the other reactions and will change comparably little in rate after ignition. It can be questioned how realistic this behavior is for the reaction and the resulting parameters are likely a product of insufficient data. The complete gas mix experiments are the only experiments in the current study where reaction 10 takes place and in these experiments it is only at very low temperatures where the reactions are identifiable (see Section 4.1). It therefore appears that the temperature dependence at higher temperature is difficult to determine with certainty which is also indicated by the large confidence interval for the parameters. The confidence intervals of the other parameters estimated are relatively small indicating that all reactions modeled, except reaction 10, were well defined by the available data. This also holds true for the effective diffusivity scaling values.

The final effective diffusivity scaling values are high for both small and large components giving effective diffusivities at 14.4 and 12.4 times the starting values calculated with the Bosanquet pore model. The model has been extensively used in pore diffusion modeling and is thoroughly described by, for example, Zalc et al. [57]. This model (Eq. (7)) includes both the Knudsen and bulk gas diffusion resistances. However, since the Knudsen diffusivity is approximately an order of magnitude lower, its value dominates the final estimated effective diffusivity. Since the scaling factors increase the diffusivity by at least an order of magnitude, it can be concluded that in fact the prevailing transport mechanism in the washcoats was bulk gas diffusion in macropores. As a reference the results are compared with a study performed by Novak et al. [18] where effective diffusion for CO was simulated based on a digital reconstruction of a similar Pt/Al_2O_3 porous layer. The comparison is shown in Fig. 12 where the reference study is compared to the estimated results from the current study at three temperature levels.

The modeled effective diffusion has a reasonable agreement with the more detailed reference model but it is also apparent

Table 4
Experiments used for modeling and validation.

Experiment Type	Cat # used for parameter estimation	Cat # used for verification
CO light-off	1,3,6	2,4,5
C_3H_6 light-off	2,5,6	1,3,4
NO oxidation light-off	1,5,6	2,3,4
Complete gas mix	2,3,6	1,4,5

Table 5
Final parameter values for tuned parameters including 95% confidence intervals. Pre-exponential factors of reaction 2, 4, 6, 8, 9 and 10 are given in mol/(kgPt,s) and remaining pre-exponential factors are given in m^3/(kgPt,s). Activation energies are given in J/mol and effective diffusivity scaling are dimensionless.

Tuned parameters					
	Value	95% confidence interval		Value	95% confidence interval
A_2	$2.08E \times 10^7$	$[1.61,2.67] \times 10^7$	$E_{A.2}$	5.61×10^4	$[5.52,5.70] \times 10^4$
A_4	1.32×10^8	$[1.18,1.48] \times 10^8$	$E_{A.4}$	5.02×10^4	$[4.98,5.06] \times 10^4$
A_5	1.70×10^5	$[1.82,1.91] \times 10^5$	$E_{A.5}$	3.39×10^4	$[3.36,3.42] \times 10^4$
A_8	6.15×10^{16}	$[4.58,8.26] \times 10^{16}$	$E_{A.8}$	1.61×10^5	$[1.60,1.63] \times 10^5$
A_9	2.05×10^{14}	$[1.78,2.36] \times 10^{14}$	$E_{A.9}$	$9{,}91 \times 10^4$	$[9.87,9.96] \times 10^4$
A_{10}	30.5	[13.4,69.5]	$E_{A.10}$	3.32×10^3	$[0.53,6.11] \times 10^3$
A_{11}	2.44×10^8	$[2.16,2.76] \times 10^8$	$E_{A.11}$	5.08×10^4	$[5.04,5.12] \times 10^4$
A_{12}	1.38×10^{13}	$[0.96,1.99] \times 10^{13}$	$E_{A.12}$	1.03×10^5	$[1.01,1.04] \times 10^5$
$f_{Dscl,S}$ †	14.4	[14.36,14.51]	$f_{Dscl,L}$ †	12.4	[12.36,12.54]
Fixed parameters					
A_1	2.49×10^6		$E_{A.1}$	2.10×10^4	
A_3	2.86×10^7		$E_{A.3}$	0	
A_6	1.33×10^{10}		$E_{A.6}$	1.25×10^5	
A_7	5.44×10^3		$E_{A.7}$	0	

† Effective diffusivity scaling for small (S) and large (L) molecules.

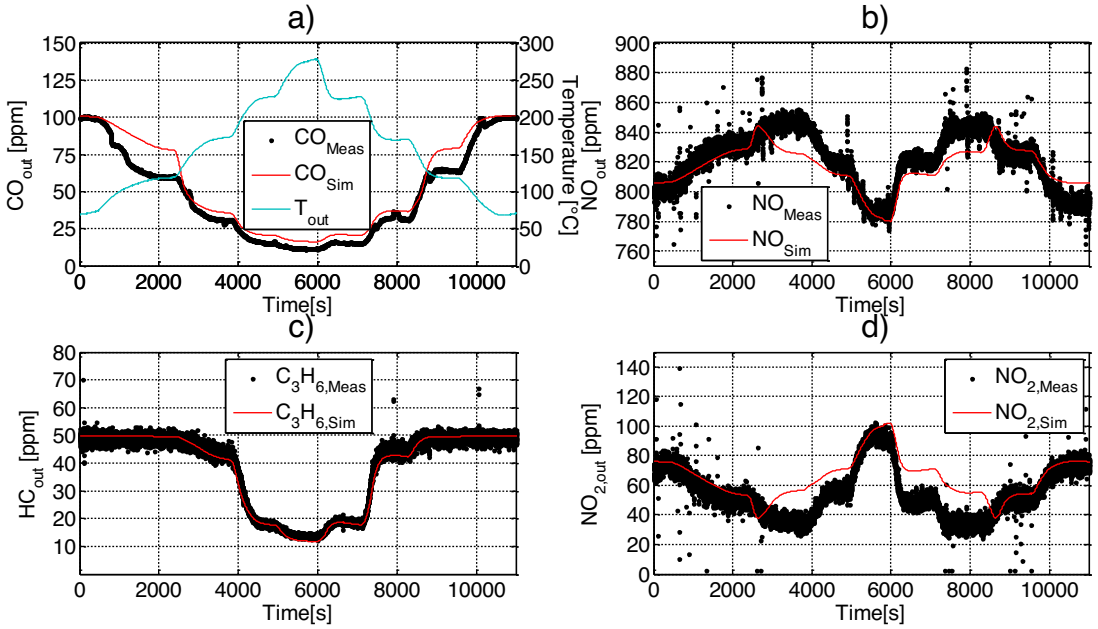

Fig. 13. Experimental and simulation results for complete gas mix for catalysts 6 with 5 g/ft^3 platinum loading and 2 g/inch^3 inert washcoat loadings. The inlet concentrations were 100 ppm CO, 800 ppm NO, 50 ppm C_3H_6 and 80 ppm NO_2.

that diffusivities in the reference model had a stronger dependence on temperature. This difference originates from the more detailed model of the pore structure in the reference case having a larger influence from diffusion in macropores that have a stronger temperature dependence [58]. The weaker temperature dependence of diffusivities in the current study stems from the dominance of Knudsen diffusion resistance in the Bosanquet pore model. However, since the final effective diffusivities were scaled-up by more than an order of magnitude into a range consistent with bulk gas diffusion, a stronger dependence on temperature may well be more appropriate. The simulation of the CO light-off experiments, however, show that the modeled effective diffusivity also resulted in a good agreement with experimental data which can be seen in Figs. 7 and 8 (panels a and b).

Fig. 7 also shows that the conversion levels are well represented but that the extinction dynamics are too fast for the modeling result. An earlier extinction in measurement data for the catalyst with lower conversion is expected but the slower dynamics is not. The slower extinction dynamics could be a result of the thermal properties of the catalyst with different inert washcoat loadings. If radial temperature gradients have an influence on the measurement data, which was speculated in the previous section about NO

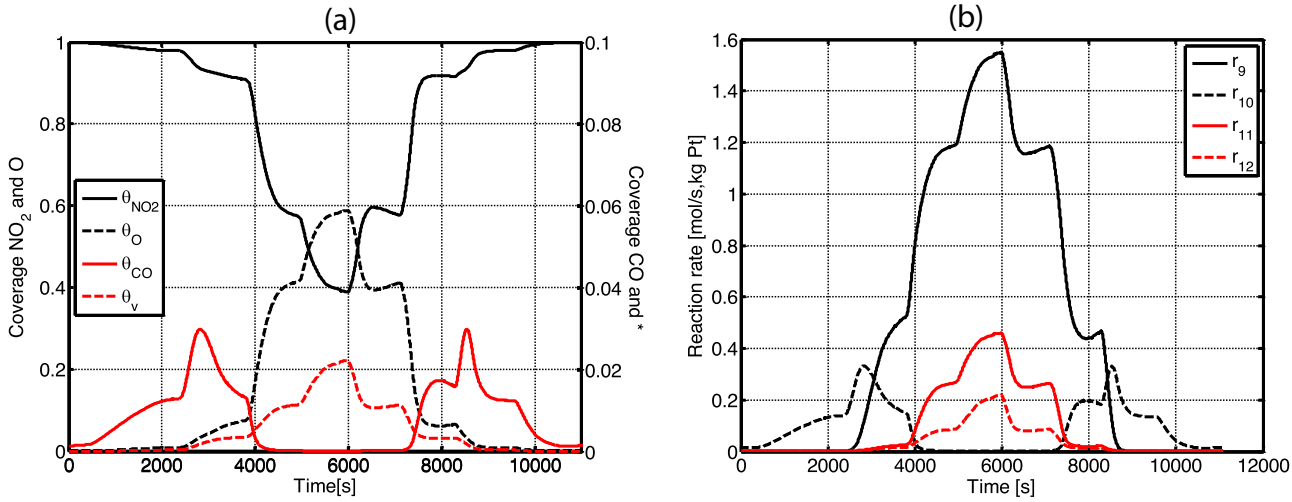

Fig. 14. Simulation results of complete gas mix experiment with catalyst 6; a) coverages, b) reaction rates for oxidation of CO and C_3H_6.

oxidation light-off hysteresis, a difference in thermal mass such as inert washcoat layer thickness may give different results for different catalysts. Radial temperature gradients are not simulated by the single channel model used here, but an improved fit to the ignition should at least be possible with the current model formulation. Fig. 8 shows a good agreement between simulation and experiments for C_3H_6 both in terms of ignition and extinction but also for conversion levels even though the simulated dynamics of ignition and extinction are somewhat slower than the measured data. The model captures the different mass transfer resistance when changing the inert washcoat layer. When considering real engine emissions, the model HC (propene) is considered to be highly reactive compared to smaller alkanes (e.g. C_3H_8 and methane) and also "small" compared with many other real exhaust hydrocarbons [59]. Since larger molecules will have lower diffusivities, the findings from this study highlights the need for improved models for internal washcoat mass transfer.

The modeling results for NO oxidation light-off are shown in Fig. 9 (panel a). In general a larger difference between simulation results and modeled data characterize the NO-light-off experiments. Since the source of the hysteresis was assumed to be related to platinum oxide formation and/or temperature gradients the model is unable to replicate the lower conversion as the temperature increases (ca. 1300 s). However, since the status of the Pt sites are likely most reproducible for the different catalysts after the heat-up period, the model displays a better fit after the maximum temperature is reached than before. This is especially clear for catalyst 2 that has the largest hysteresis. The measurement data show that both catalyst 5 and 6 reach the thermodynamic limit for NO oxidation at around 1300 s where the conversion starts to decrease even if the temperature is increasing. The conversion continues to be at the equilibrium limit until about 2250 s where the conversion again starts to decrease with decreasing temperature. Unexpectedly the conversion for catalyst 2 is about 30 ppm above the thermodynamic limit when the temperature is highest, between 1500 and 2000 s. It is however unlikely that the catalyst with the least transport resistance would not reach the equilibrium and the accuracy of the NO measurement in this experiment can therefore be questioned (it was therefore not included in the data used for parameter estimation). In the modeling results the thermodynamic equilibrium was reached between 1300 and 2250 s for catalyst 2 but not for catalyst 5 and 6 that were 30–40 ppm above the equilibrium levels.

Since simulated NO concentrations reached the equilibrium limit for the catalyst without an inert washcoat layer, but did not for the ones with the inert washcoat, the model must have overestimated the mass transport resistance of NO. Two factors that likely contribute to this shortcoming of the internal mass transfer resistance description are the effective diffusivity model and the washcoat geometrical description.

Fig. 12 showed that the more detailed reference model of effective diffusivity gave a higher effective diffusivity than the estimated model at high temperature but a lower effective diffusivity at low temperature. This may explain why the simulated transport resistance for CO and C_3H_6, that have light-off at lower temperatures, agrees better with measurement data than NO that lights off at higher temperature. A more detailed effective diffusivity model may have improved the possible final fit of the model. In addition, the washcoat structure in the model assumes square channels of uniform washcoat thickness even though the real channels are more circular with increased washcoat thickness in the corners. A more realistic model of the washcoat distribution could improve the modeling conditions by permitting a distinction between pore structure and washcoat geometry.

In Fig. 13 the simulation results from one of the complete gas mix experiments is shown. Overall the agreement between simulations and experiment is very good even though the CO concentration is somewhat higher than the measured values around 2000 s. To evaluate the kinetic model the surface coverages and the reaction rates for oxidation of CO and C_3H_6 are shown in Fig. 14.

As the analysis of the experimental data suggested in Section 4.1, NO_2 is initially the most active oxidant giving it a dominant surface presence at low temperature. This is also seen in panel b) where CO oxidation by NO_2, r_{10}, is the fastest reaction during the first (and last) 3000 s. Due to the high NO_2 coverage, the CO coverage will remain low throughout the experiment and thereby negate any CO inhibition effects. As the temperature increases the oxygen coverage increases as reactions with oxygen as oxidizing species (r_9 and r_{11}) take over as the fastest reactions. The role of C_3H_6 oxidation by NO_2 (r_{12}) is difficult to identify from the measurement data but from the simulation results it appears that the reaction becomes active at the same temperature as the regular oxidation of C_3H_6 by oxygen (r_{11}). Since CO is oxidized only by oxygen at the temperature where r_{12} is active, the reaction may be necessary to achieve NO_x concentrations that agree with the experimental data.

The main difference between the current kinetic model and the classical global kinetic model by Voltz et al. [9], on which many

recent models are based, is the inhibition by C_3H_6 and CO. In the Voltz model both C_3H_6 and CO inhibition is described by inhibition terms due to competitive adsorption. However in much of the work by Voltz et al. the concentrations of these species are much higher than the level in the exhaust for a modern lean burn engine as considered in the present study. In the current kinetic model CO inhibition by competitive adsorption was more apparent than that by C_3H_6 and in the interest of a simpler model C_3H_6 inhibition was omitted. It has been shown in experimental studies that C_3H_6 and CO also can have inhibition effects on NO oxidation due to their reaction with NO_2, however this effect is rarely included in modeling studies. Even the most detailed kinetic models that can be applied to DOC operation [50], lack pathways accounting for reactions between NO_2 and CO or hydrocarbons. In this current study with conditions comparable to modern diesel engine exhaust these inhibition effects were included in the model also meaning that CO and hydrocarbons will have an inhibiting effect on NO oxidation primarily by reaction and to a lesser degree by competitive adsorption.

The kinetic parameters were estimated with reasonable confidence intervals (as shown in Table 5) which only indicates an information-rich set of experimental data, independent of variations in the parameter sensitivities. Since there is a clear lack of fit, the model parameter values or the model as such, cannot be deemed valid and these shortcomings have been discussed above. In this study, the gradient search was halted when the residual decrease was too slow and a local minima could be suspected. Alternative parameter estimation techniques (e.g. global optimization algorithms) would probably not improve the situation and would require much longer simulation time. To our understanding, lack of fit should stem from shortcomings in the model itself concerning both the kinetics and the mass transfer. However, as pointed out on many occasions in this paper, the model has many merits and thus serves the purpose for increased mechanistic insight and for directions of further research.

5. Conclusions

The conclusions from the current study can be divided into two parts where the first part includes the conclusions from the analysis of the experiments and the second includes the conclusions from the modeling results. The light-off experiments and the complete gas mix experiment with different catalyst configurations showed that

- NO_2 is a stronger oxidizing agent than O_2 and plays an important role at low temperature (<120 °C). In a complete exhaust gas mixture, NO_2 reacts preferentially with CO rather than C_3H_6 causing an apparent inhibition of NO oxidation at low temperature.
- A clear effect of washcoat transport resistance was apparent in the data for C_3H_6 and CO but also indicated for NO.
- Inhibition effects due to competitive adsorption were more apparent for CO than for C_3H_6 at the relatively low levels studied here that are relevant for a modern lean burn engine exhaust.

In the modeling part, a reactor and kinetic model was derived involving a compromise between accuracy and computational demands. Features of the models include:

- A good agreement between simulation and measurement data was achieved with a model using O, CO and NO_2, but not hydrocarbons and NO, as surface species.
- Reactions between surface NO_2 and primarily CO were included that effectively accounted for reduced NO oxidation efficiency.
- Using different thicknesses of an inert washcoat layer closest to the gas bulk improves the conditions for resolving kinetics from transport phenomena. The final estimated values of effective diffusivity indicated that bulk gas diffusion in macropores was the prevailing transport mechanism.

Acknowledgements

The computations were performed on resources provided by the Swedish National Infrastructure for Computing (SNIC) at C3SE. Financial support from Swedish Energy Agency is gratefully acknowledged

References

[1] X. Auvray, Vehicle emission abatement: NO oxidation and ammonia SCR, Chalmers University of Technology, 2011.
[2] M.P. Harold, M.E. Garske, J. Catal. 127 (1991) 524–552.
[3] S. Salomons, R.E. Hayes, M. Votsmeier, A. Drochner, H. Vogel, S. Malmberg, J. Gieshoff, Appl. Catal. B: Environ. 70 (2007) 305–313.
[4] J.W. Chorkendorff Niemantsverdriet, Concepts of modern catalysis and kinetics, Wiley-VCH, 2003.
[5] K. Hauff, U. Tuttlies, G. Eigenberger, U. Nieken, Appl. Catal. B: Environ. 100 (2010) 10–18.
[6] Y.D. Kim, W.S. Kim, Ind. Eng. Chem. Res. 48 (2009) 6579–6590.
[7] F. Lafossas, Y. Matsuda, A. Mohammadi, A. Morishima, M. Inoue, M. Kalogirou, G. Koltsakis, Z. Samaras, SAE Int. J. Engines 4 (2011) 1586–1606.
[8] X. Song, H. Surenahalli, J. Naber, G. Parker, J. Johnson, Experimental and Modeling Study of a Diesel Oxidation Catalyst (DOC) under Transient and CPF Active Regeneration Conditions, SAE International, 2013.
[9] S.E. Voltz, C.R. Morgan, D. Liederman, S.M. Jacob, Prod. R&D 12 (1973) 294–301.
[10] K. Irani, W.S. Epling, R. Blint, Appl. Catal. B: Environ. 92 (2009) 422–428.
[11] T.J. Wang, S.W. Baek, J.H. Lee, Ind. Eng. Chem. Res. 47 (2008) 2528–2537.
[12] R.E. Hayes, S.T. Kolaczkowski, Catal. Today 47 (1999) 295–303.
[13] K. Ramanathan, V. Balakotaiah, D.H. West, AIChE J. 50 (2004) 1493–1509.
[14] A. Holmgren, B. Andersson, Chem. Eng. Sci. 53 (1998) 2285–2298.
[15] S.T. Kolaczkowski, Catal. Today 83 (2003) 85–95.
[16] F. Zhang, R.E. Hayes, S.T. Kolaczkowski, Chem. Eng. Res. Des. 82 (2004) 481–489.
[17] P. Kočí, V. Novák, F. Štěpánek, M. Marek, M. Kubíček, Chem. Eng. Sci. 65 (2010) 412–419.
[18] V. Novák, P. Kočí, M. Marek, F. Štěpánek, P. Blanco-García, G. Jones, Catal. Today 188 (2012) 62–69.
[19] V. Novák, P. Kočí, T. Gregor, J.-S. Choi, F. Štěpánek, M. Marek, Catal. Today 216 (2013) 142–149.
[20] R.E. Hayes, S.T. Kolaczkowski, Chem. Eng. Sci. 49 (1994) 3587–3599.
[21] P.S. Metkar, N. Salazar, R. Muncrief, V. Balakotaiah, M.P. Harold, Appl. Catal. B: Environ. 104 (2011) 110–126.
[22] B. Wickman, A. Lundstrom, J. Sjoblom, D. Creaser, Top. Catal. 42-43 (2007) 123–127.
[23] I. Nova, D. Bounechada, R. Maestri, E. Tronconi, A.K. Heibel, T.A. Collins, T. Boger, Ind. Eng. Chem. Res. 50 (2010) 299–309.
[24] B. Sukumar, J. Dai, A. Johansson, P. Markatou, M. Ahmadinejad, T. Watling, B. Ranganath, A. Nande, T. Szailer, Modeling of Dual Layer Ammonia Slip Catalysts (ASC), SAE Technical Paper 2012-01-1294, 2012, http://dx.doi.org/10.4271/2012-01-1294.
[25] S.B. Kang, S.J. Han, I.-S. Nam, B.K. Cho, C.H. Kim, S.H. Oh, Chem. Eng. J. 241 (2014) 273–287.
[26] A. Scheuer, W. Hauptmann, A. Drochner, J. Gieshoff, H. Vogel, M. Votsmeier, Appl. Catal. B: Environ. 111–112 (2012) 445–455.
[27] R.J. Berger, F. Kapteijn, J.A. Moulijn, G.B. Marin, J. De Wilde, M. Olea, D. Chen, A. Holmen, L. Lietti, E. Tronconi, Y. Schuurman, Appl. Cata. A: Gen. 342 (2008) 3–28.
[28] B. Lundberg, J. Sjoblom, Å. Johansson, B. Westerberg, D. Creaser, SAE int, J. Engines 7 (2) (2014) 1093–1112, http://dx.doi.org/10.4271/2014-01-9049.
[29] N. Mladenov, J. Koop, S. Tischer, O. Deutschmann, Chem. Eng. Sci. 65 (2010) 812–826.
[30] R.D. Hawthorn, AIChE Symp. Ser. 70 (1974) 11.
[31] J. Sjoblom, D. Creaser, Comput. Chem. Eng. 32 (2008) 3121–3129.
[32] L. Boyang, O. Yew-Soon, L. Minh Nghia, G. Chi Keong, Memetic gradient search, evolutionary computation, 2008. CEC 2008. (IEEE world congress on computational intelligence), IEEE Congress on (2008) 2894–2901.
[33] B. Lundberg, J. Sjöblom, Å. Johansson, B. Westerberg, D. Creaser, Comput. Chem. Eng. 74 (2015) 144–157.
[34] K. Hauff, U. Tuttlies, G. Eigenberger, U. Nieken, Appl. Catal. B: Environ. 123–124 (2012) 107–116.
[35] K. Hauff, H. Dubbe, U. Tuttlies, G. Eigenberger, U. Nieken, Appl. Catal. B: Environ. 129 (2013) 273–281.
[36] W. Hauptmann, M. Votsmeier, J. Gieshoff, A. Drochner, H. Vogel, Appl. Catal. B: Environ. 93 (2009) 22–29.

[37] T. Watling, M. Ahmadinejad, M. Ţuţuianu, Å. Johansson, SAE int, J. Engines 5 (3) (2012) 1420–1442, http://dx.doi.org/10.4271/2012-01-1286.
[38] A. Arvajová, P. Kočí, V. Schmeißer, M. Weibel, Appl. Catal. B: Environ. 181 (2016) 644–650.
[39] S. Salomons, M. Votsmeier, R.E. Hayes, A. Drochner, H. Vogel, J. Gieshof, Catal. Today 117 (2006) 491–497.
[40] A.M. Stamatelos, G.C. Koltsakis, I.P. Kandylas, G.N. Pontikakis, Proceedings of the institution of mechanical engineers, part d, J. Automobile Eng. 213 (1999) 545–560.
[41] G.P. Ansell, P.S. Bennett, J.P. Cox, J.C. Frost, P.G. Gray, A.M. Jones, R.R. Rajaram, A.P. Walker, M. Litorell, G. Smedler, Appl. Catal. B: Environ. 10 (1996) 183–201.
[42] A. Pandya, J. Mmbaga, R.E. Hayes, W. Hauptmann, M. Votsmeier, Top. Catal. 52 (2009) 1929–1933.
[43] M. Khosravi, A. Abedi, R.E. Hayes, W.S. Epling, M. Votsmeier, Appl. Catal. B: Environ. 154–155 (2014) 16–26.
[44] M. Khosravi, C. Sola, A. Abedi, R.E. Hayes, W.S. Epling, M. Votsmeier, Appl. Catal. B: Environ. 147 (2014) 264–274.
[45] S.H. Oh, J.C. Cavendish, Ind. Eng. Chem. Prod. Res. Dev. 21 (1982) 29–37.
[46] L. Olsson, B. Westerberg, H. Persson, E. Fridell, M. Skoglundh, B. Andersson, J. Phys. Chem. B 103 (1999) 10433–10439.
[47] J.M.A. Harmsen, J.H.B.J. Hoebink, J.C. Schouten, Studies in Surface Science and Catalysis, in: G.F. Froment, K.C. Waugh (Eds.), Elsevier, 2001, pp. 349–356.
[48] X. Li, M. Meng, P. Lin, Y. Fu, T. Hu, Y. Xie, J. Zhang, Top. Catal. 22 (2003) 111–115.
[49] M. Crocoll, S. Kureti, W. Weisweiler, J. Catal. 229 (2005) 480–489.
[50] J. Koop, O. Deutschmann, Appl. Catal. B: Environ. 91 (2009) 47–58.
[51] D. Bhatia, R.W. McCabe, M.P. Harold, V. Balakotaiah, J. Catal. 266 (2009) 106–119.
[52] S.S. Mulla, N. Chen, W.N. Delgass, W.S. Epling, F.H. Ribeiro, Catal. Lett. 100 (2005) 267–270.
[53] W. Hauptmann, A. Drochner, H. Vogel, M. Votsmeier, J. Gieshoff, Top. Catal. 42-43 (2007) 157–160.
[54] R. Burch, D. Ottery, Appl. Catal. B: Environ. 9 (1996) L19–L24.
[55] R. Burch, D. Ottery, Appl. Catal. B: Environ. 13 (1997) 105–111.
[56] D. Chatterjee, O. Deutschmann, J. Warnatz, Faraday Discuss. 119 (2002) 371–384.
[57] J.M. Zalc, S.C. Reyes, E. Iglesia, Chem. Eng. Sci. 59 (2004) 2947–2960.
[58] M. Dudák, V. Novák, P. Kočí, M. Marek, P. Blanco-García, G. Jones, Appl. Catal. B: Environ. 150–151 (2014) 446–458.
[59] J. Mattson, R. O'Malley, C., Depcik, E. Peltier, SAE Technical Paper 2013–01-1348, 2013, 10.4271/2013–01-1348.